AGU PUBLICATIONS

JGR

Journal of Geophysical Research: Space Physics

RESEARCH ARTICLE
10.1002/2014JA020823

Key Points:
- During the solar flare occurrence, the TEC disturbance is larger at the EIA crest
- At the flare initiation, the electron density increases faster at low altitudes
- At half an hour after the flare, the *F* region electron density increase dominates

Correspondence to:
P. A. B. Nogueira,
paulo.nogueira@inpe.br;
pauloabn@hotmail.com

Citation:
Nogueira, P. A. B., et al. (2015), Modeling the equatorial and low-latitude ionospheric response to an intense X-class solar flare, *J. Geophys. Res. Space Physics*, *120*, doi:10.1002/2014JA020823.

Received 18 NOV 2014
Accepted 8 MAR 2015
Accepted article online 11 MAR 2015

Modeling the equatorial and low-latitude ionospheric response to an intense X-class solar flare

P. A. B. Nogueira[1], J. R. Souza[1], M. A. Abdu[1], R. R. Paes[1], J. Sousasantos[1], M. S. Marques[1], G. J. Bailey[2], C. M. Denardini[1], I. S. Batista[1], H. Takahashi[1], R. Y. C. Cueva[3], and S. S. Chen[1]

[1]Divisão de Aeronomia, Instituto Nacional de Pesquisas Espaciais, São José dos Campos, Brazil, [2]Department of Applied Mathematics, University of Sheffield, Sheffield, UK, [3]Instituto Presbiteriano Mackenzie, Escola de Engenharia, Universidade Presbiteriana Mackenzie, São Paulo, Brazil

Abstract We have investigated the ionospheric response close to the subsolar point in South America due to the strong solar flare (X2.8) that occurred on 13 May 2013. The present work discusses the sudden disturbances in the *D* region in the form of high-frequency radio wave blackout recorded in ionograms, the *E* region disturbances in the form of the Sq current and equatorial electrojet intensifications, and the enhancement and decay in the ionospheric total electron content (TEC) as observed by a network of Global Navigation Satellite Systems receivers, the last of these manifestations constituting the main focuses of this study. The dayside ionosphere showed an abrupt increase of the TEC, with the region of the TEC increase being displaced away from the subsolar point toward the equatorial ionization anomaly (EIA) crest region. The decay in the ΔTEC following the decrease of the flare EUV flux varied at a slower ratio near the EIA crest than at the subsolar point. We used the Sheffield University Plasmasphere-Ionosphere Model to simulate the TEC enhancement and the related variations as arising from the flare-enhanced solar EUV flux and soft X-rays. The simulations are compared with the observational data to validate our results, and it is found that a good part of the observed TEC variation features can be accounted for by the model simulation. The combined results from model and observational data can contribute significantly to advance our knowledge about ionospheric photochemistry and dynamics needed to improve our predictive capability on the low-latitude ionospheric response to solar flares.

1. Introduction

A solar flare is characterized as a sudden and intense but relatively short-lived increase in the brightness, observed over the Sun's surface or solar limb. The flare arises when the magnetic energy accumulated in the Sun's atmosphere is abruptly released. Radiation is emitted across the entire electromagnetic spectrum and more notably in the spectral region from X-ray to solar extreme ultraviolet (EUV). The EUV and X-ray flares are responsible for enhanced ionization in the Earth's ionospheric *D*, *E*, and *F* regions, with potential impact in space-based communication and navigation systems. The EUV radiation is absorbed at higher altitudes, heating and ionizing the *E* and *F* regions [see, for example, *Xiong et al*., 2011; *Tsurutani et al*., 2005; *Manju et al*., 2009]. The X-rays that penetrate more deeply into the atmosphere enhance the *D* region electron density causing short radio wave blackout as that detected in ionograms [*Sripathi et al*., 2013], and the lowering of reflection height and phase advance at very low frequency (VLF) [see, for example, *Raulin et al*., 2013]. Many authors have previously studied the ionospheric response to solar flares in the last decades. Nevertheless, it still remains as an important research field in ionospheric physics, mainly considering the possibility to improve the capacity and reliability of predicting disturbances in space weather [*Van Sabben*, 1968; *Thome and Wagner*, 1971; *Rangarajan and Rastogi*, 1981; *Liu et al*., 1996; *Afraimovich et al*., 2001; *Xiong et al*., 2011]. There is also an increasing interest in theoretical modeling of the ionospheric impact to solar flare events [*Le et al*., 2007; *Qian et al*., 2010, 2012].

The increase in the electromagnetic emission flux during solar flare events is always accompanied by geomagnetic field disturbances, whose signature in ground magnetograms has often been known as "*crotchet*." Such behavior has been studied by *Moldavanov* [2002] and may be understood as sudden changes in geomagnetic field parameters (recorded in magnetograms) due to the sudden intensification in the global ionospheric current system caused by the flare-induced enhanced ionospheric conductivity.

Table 1. Geographic Coordinates of Ground Stations

	Latitude (deg)	Longitude (deg)	Dip Angle (deg)	Instrumentation
São Luís	−2.60	−44.21	−6.1	Magnetometer Digisondes GNSS receiver
Jicamarca	−11.95	−76.87	0.13	Magnetometer
Piura	−5.17	−80.64	12.68	Magnetometer
Cachoeira Paulista	−22.6	−45.0	−35.39	Magnetometer
Rio Grande	−53.75	−67.75	−51.51	Magnetometer
Eusébio	−3.89	−38.44	−14.83	Magnetometer
Fortaleza	−3.92	−38.48	−14.84	Digisondes
Atibaia	−23.18	−46.6	−34.72	SAVNET
Belém	−1.4	−48.45	0.79	GNSS receiver
Palmas	−10.15	−48.33	−14.70	GNSS receiver
Barreiras	−12.15	−45	−21.45	GNSS receiver

Sripathi et al. [2013] have discussed a case of an abrupt increase in the ionospheric total electron content (TEC) due to the enhancement of the EUV flux, accompanied by the sudden disappearance of ionogram echoes caused by intense *D* region absorption of high-frequency (HF) radio waves during an X-class solar flare event (which represents values of the X-ray flux (1–8 Å) larger than 10^{-4} W/m^2).

In the present work, we analyze the responses of the ionospheric *D*, *E*, and *F* regions during the solar flare event that occurred near midday on 13 May 2013. This solar flare was classified as an X2.8 class event, the second strongest in 2013, and occurred at the Sun's eastern limb. Using VLF propagation paths, we observed *D* region ionization increase that also caused a shortwave radio blackout as inferred from ionograms registered at equatorial stations [see also *Rastogi et al*., 1999; *Thomson et al*., 2004; *Thomson and Clilverd*, 2001]. Here we have analyzed the Digisonde and magnetometer data from Brazilian and Peruvian equatorial and low-latitude sites for a quick evaluation of the flare manifestations in the *D* and *E* regions of the ionosphere. The main aim of the present work is, however, to perform a quantitative evaluation of the TEC disturbance during this flare event in the equatorial and low-latitude ionosphere close to midday. For this purpose, we have analyzed the TEC data obtained from a netwok of Global Navigation Satellite System (GNSS) receivers in South America. Additionally, we have modeled the TEC variations produced by the flare-enhanced X-ray and EUV fluxes using the Sheffield University Plasmasphere-Ionosphere Model (SUPIM). For a detailed description of SUPIM, see *Bailey et al*. [1993] and *Bailey and Balan* [1996]. We show that the flare-induced TEC enhancements and the associated electron density altitudinal and latitudinal distributions can be explained by a theoretical model simulation that uses the EUV and X-ray fluxes as obtained from satellite observations. The study is performed with the purpose of characterizing the equatorial ionization anomaly response to transient increases of ionizing radiations during a solar flare in the South American longitude sector. We present in section 2 the methodology to obtain the variations in ΔH, the horizontal component of the Earth's magnetic field, representing the Sq and equatorial electrojet (EEJ) current systems, the TEC calculation, and the ionospheric simulation procedure using SUPIM. Section 3 deals with the results of analysis of the observational data and of SUPIM simulation runs and discussion of the results, and section 4 presents a summary and the conclusions.

2. Methodology

2. 1. The ΔH Variations Representing the Sq and EEJ Current Strength

One minute resolution data of the geomagnetic field horizontal component (*H*) variations over Eusébio (slightly off equator), Cachoeira Paulista (low latitude), Rio Grande (midlatitude), Jicamarca (magnetic equator), and Piura (slightly off equator) were used to obtain the ΔH index values, by subtracting the midnight values of the *H* component, considered as baseline values, from the *H* field at other local times. This procedure serves to eliminate the contribution due to the Earth's main field, in the diurnal variation of the *H* field, leading to the ΔH variations due to the Sq current system. To calculate the EEJ strength, which we have done for the Peruvian sector, the ΔH variation at an off-equator station, Piura (in this case), was subtracted from that over the dip equatorial station, Jicamarca. Table 1 shows the geographic coordinates and the magnetic inclination for all the ground stations used in the present work.

2.2. GNSS TEC Variation, ΔTEC, and ΔTEC/Δ*t*

The dual-frequency radio signals from the Global Navigation Satellite Systems (GNSS) allow measurements of the total number of electrons in a column of unit cross-section area, called total electron content (TEC), along the raypath from GNSS satellite to a receiver. A number of GNSS ground-based receiver networks to monitor the TEC are operated in South America. These networks are the following: RAMSAC (Rede Argentina de Monitoreo Satelital Continuo, 36 stations), LISN (Low-Latitude Ionospheric Sensor Network, 27 stations), RBMC (Rede Brasileira de Monitoramento Contínuo, 87 stations), and IGS (International GNSS Service, 25 stations). The Brazilian Space Weather program routinely generates TEC maps over South America using a methodology developed by *Otsuka et al*. [2002].

For this study we have obtained two-dimensional maps of the absolute vertical TEC values at 10 min time resolution and 0.5°×0.5° of spatial resolution in latitude and longitude. We have also derived the TEC values for individual station at a time resolution of 30 s. The map of the TEC enhancement due to the solar flare (the ΔTEC map) was obtained by calculating the difference between the TEC map for the flare day and the TEC map for the previous day that happened to be a geomagnetic quiet day. We would expect the ΔTEC values to be close to zero during the whole day, except during the period of the solar flare when the increase in the ion production occurred. This technique allows us to observe the transient increases in the ionospheric electron density at 10 min running interval. We have applied the same methodology to obtain the TEC disturbances for each single station.

In addition, we have calculated also the rate of the TEC variations associated with the enhanced EUV flux during the solar flare. For this, the time rate of change of TEC was estimated as $\frac{\Delta \mathrm{TEC}}{\Delta t} = \frac{\mathrm{TEC}(t+\Delta t)-\mathrm{TEC}(t)}{\Delta t}$, ($\Delta t = 30$ s), which can show how fast the TEC is changing due to the solar flare event.

2.3. Model Simulations by SUPIM

SUPIM is a theoretical two-dimensional model that solves the time-dependent equations of continuity, momentum, and energy balance along magnetic field lines. The present model provides representations of the densities, field-aligned velocities, and temperatures of the ions and electron in the ionosphere and plasmasphere [*Bailey et al*., 1978, 1993; *Bailey and Sellek*, 1990; *Bailey and Balan*, 1996]. The International Geomagnetic Reference Field model was used to represent the Earth's magnetic field in SUPIM as an eccentric-dipole representation. The photochemistry in the model includes the ion production due to the solar EUV radiation varying with local time, the ion production and loss due to chemical reactions, thermal conduction, photoelectron heating, frictional heating, and local heating/cooling mechanisms. The transport effects in the SUPIM include those due to the ambipolar diffusion and thermal diffusion, ion-ion and ion-neutral collisions, thermospheric neutral winds, and vertical plasma drift [*Bailey et al*., 1997; *Bailey and Balan*, 1996; *Souza et al*., 2000]. The NRLMSISE-00 neutral atmospheric model is used as input in SUPIM to represent the neutral temperature and the neutral gas concentrations [*Picone et al*., 2002]. The solar ionizing radiation fluxes input to the model under quiet conditions are those of the solar EUV at 39 wavelength groups (from 1.86 to 105.00 nm) from the SOLAR 2000 model [*Tobiska et al*., 2000].

The simulation of the ionospheric electron density response to the solar flare radiation was carried out as follows: To represent the observed background solar EUV flux input in the model, we adopted the fluxes as obtained from the Extreme Ultraviolet Variability Experiment (EVE) on the Solar Dynamics Observatory (SDO) [*Woods et al*., 2010]. The values of the radiation fluxes taken 1 h before the solar flare onset were set as the background level, and the radiation fluxes during the course of the flare were obtained from EVE satellite data for wavelengths ranging from 1.86 nm up to 40 nm. For wavelength higher than 40 nm, for which we have no satellite information, the radiation during the flare event was obtained by multiplying the background level by a time-varying coefficient (up to 10% of background values).

3. Results and Discussion

3.1. The Solar Flare X-ray Flux and the *D* and *E* Layer Responses

The active region AR1748 erupted first during the early hours on 13 May 2013, with three consecutive X-class events occurring in less than 24 h. The first one was an X1.7-class eruption with peak at 02:17 UT, which was followed by an X2.8-class flare (focused in this study) that peaked at 16:05 UT, and the third one was an X3.2-class flare that peaked at 01:17 UT on 14 May. The AR1748 was located at N11E85 (solar coordinates),

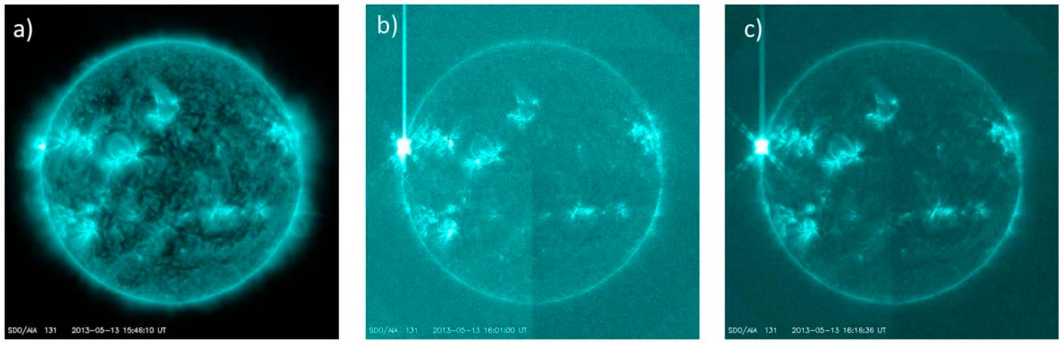

Figure 1. Satellite images illustrating the solar flare event on 13 May 2013. (a–c) The illustrative sequence obtained from SDO/AIA 133 Å at 15:46 UT, 16:01 UT, and 16:16 UT, respectively. Courtesy of NASA/SDO and the AIA, EVE, and HMI science teams.

close to the solar edge, which implies that the impact on the Earth's ionosphere would be smaller than if the emission region were closer to the solar disk center [*Liu et al.*, 2006]. Figures 1a–1c illustrate the X2.8 class flare obtained from the SDO/Atmospheric Imaging Assembly (AIA) at 133 Å. It can be observed that at 15:46 UT (Figure 1a), no flare had occurred. At 16:01 UT (Figure 1b) and at 16:16 UT (Figure 1c), the flare at the solar eastern limb may be observed. We can also note that at Figure 1b, the image was saturated due to the strong brightness.

Figure 2 shows the X-ray flux variation on 13 May 2013 (red curve) recorded by the Geostationary Operational Environmental Satellite (GOES 15). In the X-ray flux, we can clearly observe two of the mentioned solar flares. The first flare (X1.7) occurred at 02:17 UT that was on the nightside for Brazil. The second event (X2.8 class) started at 15:48 UT, peaked at 16:05 UT, and ended at 16:16 UT when it was just past midday over Brazil, the corresponding local standard time (LT = UT − 3) being 12:48 LT, 13:05 LT, and 13:16 LT, respectively. (For more details about solar flares, see *Benz* [2008]). We call attention to the ΔH variations plotted together with the X-ray flux variation. The ΔH variations during daytime are shown for Eusébio (EUS) (black line), Cachoeira Paulista (CXP) (gray line), and Rio Grande (RGA) (blue line).

We may note contrasting responses of the Sq current variations at locations increasing in latitude from the magnetic equator. Both the ΔH_{EUS} and ΔH_{CXP} show a clear diurnal variation characterized by an increase during the prenoon sector, indicative of an increasing eastward current, up to local midday when it reaches a peak of ~65 nT at Eusébio and of ~60 nT at Cachoeira Paulista, after which it shows a slow decrease in the afternoon, a behavior characteristic of the expected Sq current variations [*Heelis*, 2004] at these locations. In contrast to this, the ΔH variation over Rio Grande has an opposite (negative) trend since this station is located southward of the Sq current focus, where the return current flows westward [*Matsushita*, 1969].

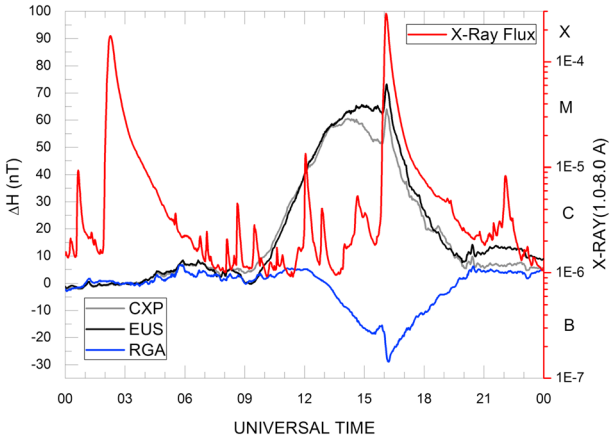

Figure 2. Daily variation of ΔH over near equator (black line), low latitude (gray line), and midlatitude (blue line). The red line shows the X-ray flux obtained from GOES satellite.

It is interesting to note that there is a sudden change (disturbance) in the ΔH at all the stations, which is coincident with the start of the solar flare; the ΔH at low-latitude stations shows a strong and rapid increase, while at midlatitude, it presents an abrupt decrease in magnitude. This sudden geomagnetic field disturbance, which occurs in the same direction that of the preflare Sq (*H* component) current, can be understood as a geomagnetic signature of the global ionospheric current system intensification, showing that the crochet current system was mostly a sudden augmentation of the Sq current, due to the sudden conductivity enhancement, caused by the flare X-ray

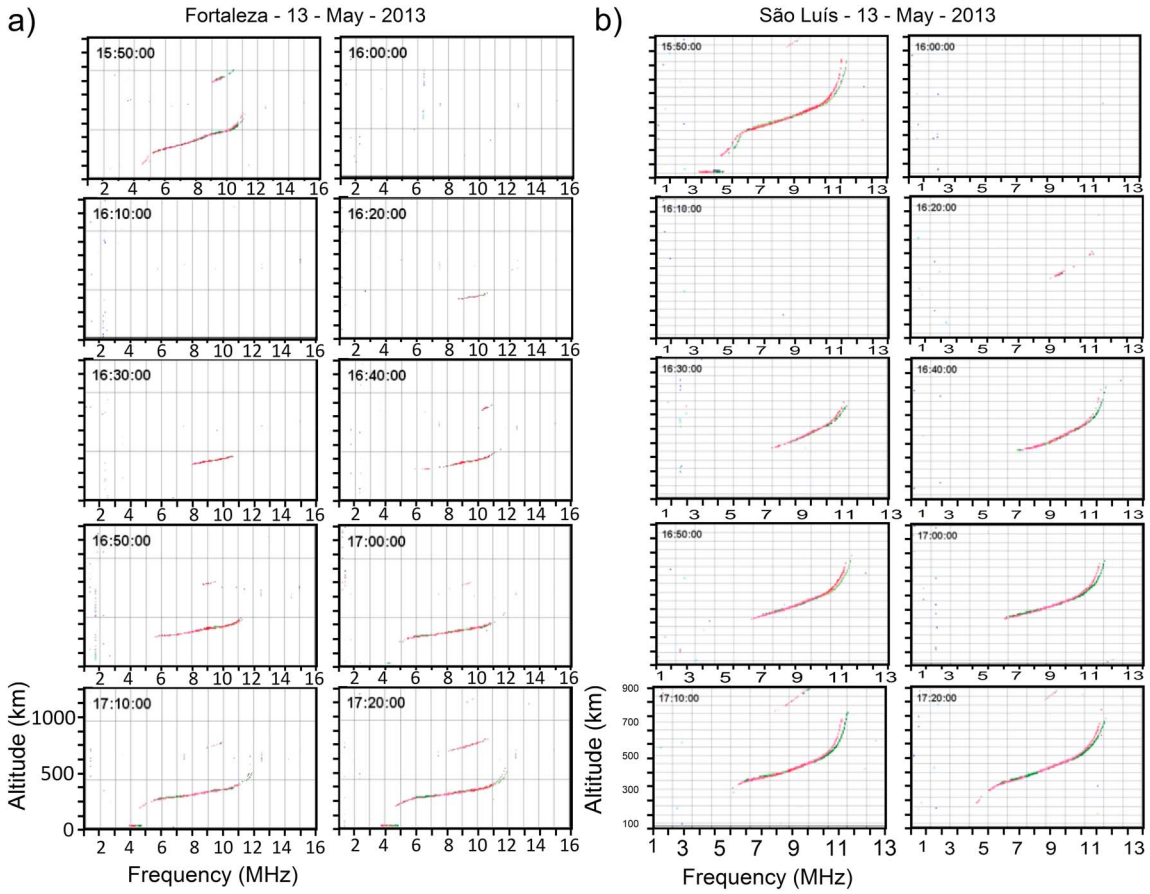

Figure 3. The sequential ionograms at 10 min interval recorded from 15:50 UT to 17:20 UT on 13 May 2013 (solar flare day) at São Luís and Fortaleza. This period covers the start, peak intensity, and decay (incomplete) of the flare X-ray flux variation. The total or partial blackout of HF wave trace can be noted in the ionograms.

ionization [see also *Rastogi et al*., 1999]. The positive response in ΔH at EUS and CXP with its simultaneous negative response at RGA is a clear demonstration that the solar flare additional ionization causes strong enhancement in the entire Sq current system.

The most directly observed ionospheric effect due to the solar flare X-ray burst is the sudden increase in the electron densities of the *D* and *E* regions of the ionosphere. The VLF signal amplitude got amplified during this solar flare event (not shown), and it may be used as indicative of the enhancement of the *D* region electron density. The enhanced *D* region ionization can also lower the VLF radio wave reflection height, causing phase advances of the received VLF signal phase. The observations of *D* region absorption in the ionograms at the same time as the VLF phase advance are an indication that the enhanced *D* region ionization was caused by the flare X-rays (see more in *Rastogi et al.* [1999], *Thomson et al*. [2004], and *Thomson and Clilverd* [2001]). The *D* region radio wave absorption and hence blackout of the ionospherically propagating short waves can be noted in the ionogram signatures presented in Figure 3 for Fortaleza and São Luís. We may notice that an increase in the f_{min} (the minimum frequency of the echo trace observed in the ionogram), which is indicative of the ionization enhancement due to the flare X-rays, was first detected in the ionogram at 15:50 UT over Fortaleza (f_{min} increased to 4.5 MHz). At São Luís located some 600 km westward Fortaleza, the effect was weaker at this time (with the $f_{min} = 3.2$ MHz only). In the subsequent ionograms at 16:00 UT and 16:10 UT, the ionograms at both the sites showed total blackout of the echoes in the entire frequency range, which coincided with the peak in the X-ray flux, as can be verified in Figure 2. With the decay in the X-ray flux that set in by ~16:20 UT, the ionogram blackout became partial, with the major recovery occurring in the ionogram at 17:10 UT (indicated by the reappearance of the *E* layer trace) over Fortaleza. The recovery over São Luís appears to be lagging behind that over Fortaleza, as it was the case also in the onset sequence of the effect. We believe that this time difference, consistently observed in the sequences of the onset

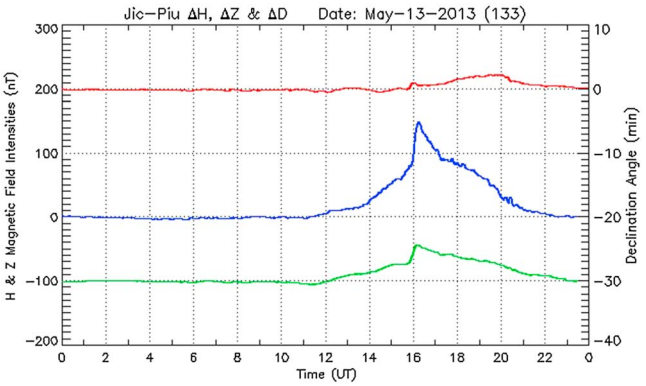

Figure 4. The blue line shows the ΔH variation, the eastward equatorial electrojet current strength; the red and green lines show, respectively, the variations in the magnetic declination and the vertical component of the magnetic field. For the Peruvian meridian, the relation between universal and local time is UT = LT + 5.

and recovery of the flare effect, which is reported here for the first time, must be due to the east-west separation of the observing sites.

An understanding of the condition for shortwave radio propagation via ionosphere, and its blackout during solar flare events resulting in difficulties for communication agencies, is an important objective of the ionospheric space weather investigations. *Sahai et al.* [2006] observed 6 h of blackout (total or partial) in ionospheric sounding observation during the solar flare event (X17.2 class flare) of 28 October 2003. In the present case of the X2.8 class flare, we observed 70 min of total or partial radio fadeouts in the Brazilian longitudes.

We now examine the solar flare-induced enhancement in the EEJ current strength in the Peruvian longitude sector (the corresponding local standard time is LT = UT − 5). For this, the ΔD, ΔH, and ΔZ variations over Piura are subtracted from their corresponding variations at Jicamarca, and the results are shown as red, blue, and green curves, respectively, in Figure 4. The diurnal variations in ΔH (the EEJ strength) and ΔZ are characterized by almost constant value close to zero before sunrise, changing to a steady increase in the morning sector to reach a maximum near midday followed by a gradual decrease toward sunset. The sudden change in all the three parameters near 16:00 UT (11:00 LT) marks the response of the EEJ to the flare X-ray irruption. The increase in the ΔH is on the order of 65 nT, which is very significant compared to the diurnal amplitude of the quiet time ΔH on this day that was around 90 nT. It is interesting to notice that the peak in the EEJ intensity occurred a few minutes (~10 min) later than the time of the peak in the X-ray flux. This delay can be interpreted as the response time of the EEJ current determined by that of the *E* layer ionizations due to a sudden increase in the ionizing X-ray flux. Interestingly, such a clear delay time is not observed in the case of the ΔZ and ΔD. We further note, comparing the results in Figures 2 and 4, that the solar flare-induced current intensity as measured by the change in ΔH is around 5 times stronger in the EEJ than that at the off-EEJ locations, which is compatible with the factor of increase expected from enhancement in the Cowling conductivity in the EEJ [*Abdu*, 2005; *Richmond*, 1995].

Several studies have reported on solar flare effects in the EEJ under the condition of counter electrojet [*Rastogi et al*., 1999; *Manju and Viswanathan*, 2005; *Manju et al*., 2009; *Sripathi et al*., 2013, and references therein]. The present results on the EEJ, using the magnetometer data from Peruvian sector, however, highlights the case of an eastward EEJ intensification instead of a counter electrojet. We have also analyzed the ΔH variation for a few other ground stations in the sunlit hemisphere for this flare event. Two of these stations are equatorial stations, three low-latitude stations, and three midlatitude stations. The results (not discussed here) showed that every equatorial and low-latitude station presented a sudden positive disturbance in the ΔH variation, and every midlatitude station presented a negative disturbance in the *H* component signatures, in agreement with the results shown in Figure 2.

3.2. The TEC Response to the Solar Flare EUV Variations

Total electron content calculated from the GNSS ground receivers showed a remarkable variation at equatorial and low-latitude locations over South America during the solar flare event. *Tsurutani et al.* [2005] reported that the dayside ionosphere responds dramatically to the X-ray and EUV emissions, with an abrupt increase in TEC, which may vary strongly depending on each flare.

Figure 5 shows the temporal variation of the EUV and TEC parameters during 15:00–17:00 UT for two ground stations. At São Luís, the TEC was measured by using pseudorandom noise (PRN) 29 (Figure 5a) and at Barreiras by using PRN 18 (Figure 5b). The EUV flux (26–34 nm wavelengths) is shown as a blue curve in

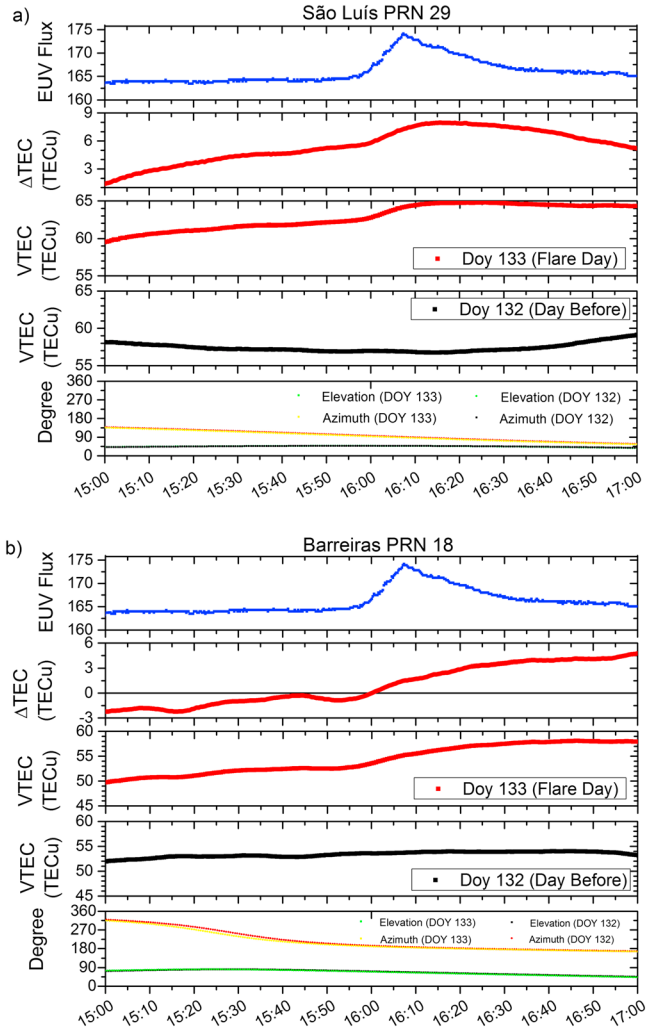

Figure 5. (first panel) EUV flux variation, followed by the (second panel) ΔTEC background removed, (third panel) the TEC variation for the flare day and (fourth panel) the day before, and (fifth panel) elevation and azimuth angle of the GNSS satellite. Figure 5a is illustrating the TEC variation over São Luís, and Figure 5b is representing Barreiras.

the first panel in Figure 5. The second panel shows ΔTEC, that is, the TEC on the flare day from which the TEC of the previous day was subtracted ($\Delta TEC = TEC_{flare\ day} - TEC_{day\ before}$). The TEC on the flare day is shown in the third panel, and the TEC on the day before (chosen to represent a quiet day) is shown in the fourth panel. Finally, in the fifth panel, we show the satellite elevation and azimuth angles on the flare day and the day before. Since the azimuth and elevation angles at the flare day and at the day before are approximately the same, the observational results on these 2 days refer to approximately the same location (similar subionospheric point), making it possible to compare the TEC differences between these days.

It can be easily observed that on the day before the flare, the TEC shows an almost flat variation (Figure 5, fourth panel), and no disturbance in TEC is present at either of the stations. However, at the time when EUV (first panel) shows a prominent increase (starting before ~16:00 UT), the TEC at both stations shows a steady growth (third panel). In the second panel showing the ΔTEC values, obtained by subtracting the quiet day vertical TEC (VTEC) values of the fourth panel from the VTEC values in the third panel, we clearly observe a rapid increase in ΔTEC at both stations. It is found that the ΔTEC over São Luís reaches its maximum values around 16:15 UT, while over Barreiras, there is a prolonged ΔTEC increase up to 17:00 UT. These TEC increases are clear evidence of the increased ion production due to the flare associated with EUV flux enhancement.

In order to have a broader view of the solar flare effect on TEC over South America, we calculated the ΔTEC for each satellite being tracked, for elevation angle above 30°. The map of ΔTEC shown in Figure 6 represents the latitude-longitude distribution of the TEC difference between the flare day (13 May) and a nonflare day (12 May 2013, which was a geomagnetic quiet day). Eight ΔTEC maps in sequence at 10 min interval are shown from 15:40 UT to 16:50 UT in this figure. The color coding depicts the ΔTEC scale ranging from −15 up to 20 total electron content unit (TECU; 1 TECU = 10^{16} el m^{-2}). The dashed line running longitudinally represents the magnetic equator. As it is to be expected, the ΔTEC before the flare onset (15:40 UT) is close to zero in a general way. Starting at 15:50 UT, the solar flare event initiation, a strong ΔTEC enhancement started to develop, that is clearly observed in the ΔTEC distribution in the map at 16:00 UT, which is close to the solar flare peak time. We note, especially, that there is a pronounced ΔTEC increase in the low-latitude region south of the magnetic equator. But this is at a longitude region where we have very limited data from the northern hemisphere. It is remarkable that the region of highest TEC increase is displaced significantly away from the subsolar point (which is close to the equator) toward

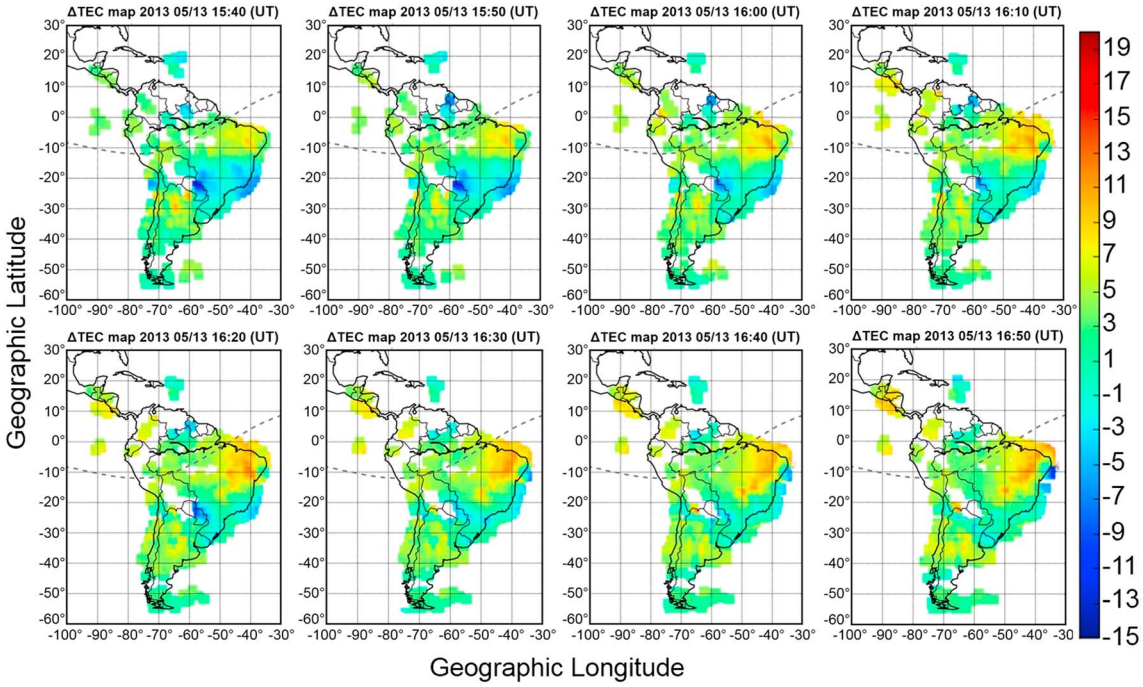

Figure 6. Longitude versus latitude distribution of the ΔTEC over South America at 10 min interval covering the period of the solar flare event.

the low-latitude region of the equatorial ionization anomaly crest in the TEC (which is near 11° off the magnetic equator [*Nogueira et al.*, 2013a]). It is also interesting to note that changes in TEC shows a significant longitudinal variation, the largest TEC increase occurring at the eastern sector of South America.

We also calculated the time rate of change of the TEC for individual PRN of the GNSS satellite passes as $\Delta TEC/\Delta t$, which is shown in Figure 7 for Belém (PRN14), São Luís (PRN29), Palmas (PRN31), and Barreiras (PRN 18); Δt used in the calculations was 30 s. We can observe that before the flare, all the receivers were showing TEC increase ratio less than 10 TECU/h. With the start of the flare as seen in the rapid rise in the X-ray flux at 15:50 UT (blue line), the TEC increase rate has promptly risen to values larger than 10 TECU/h, shows a remarkable increase until 16:00 UT, and finally goes back to the preevent level. It is interesting to note that the TEC rate of increase for each station change from a few units of ΔTEC/h up to more than 10 ΔTEC/h. We may note that at the magnetic equatorial stations (Belém and São Luís), the TEC rate of change drops to zero immediately after the solar flare occurrence time. However, at locations close to the southern crest of the EIA (Barreiras), the recovery phase (to zero values of ΔTEC/h) occurs very slowly and presents some oscillations. It seems that near the southern EIA crest, the plasma density perturbation due to flare remains for longer time (in agreement to the TEC maps in Figure 6 at 16:40 UT and 16:50 UT).

In order to explain what is driving the TEC disturbances, we used SUPIM to model the low-latitude TEC distribution. The normal inputs to SUPIM are the solar EUV fluxes for 39 wavelength bands (from 1.86 up to 105.00 nm) from SOLAR 2000 [*Tobiska et al.*, 2000], the zonal electric field from *Scherliess and Fejer* [1999], and the horizontal thermospheric neutral wind as per the horizontal wind model 93 [*Hedin et al.*, 1996]. The values of the radiation at 1 h before the solar flare onset were set as the background level, and the radiation during the flare course (15:00–17:00 UT) were obtained from EVE satellite data for wavelength bands from 1.86 nm up to 40 nm. For wavelength larger than 40 nm (for which we have no satellite data), we used the radiation flux during the course of the flare as the background level that is multiplied by a time-varying coefficient (up to 10% of the background values).

Figure 8 shows the results of SUPIM runs to calculate the TEC variation at São Luís caused by the increased EUV flux. In Figure 8 (top), the black curve shows the TEC simulation for a nonflare condition and the red curve shows the TEC simulation after including the increased flare EUV flux. Removing the baseline reference (black curve) from the disturbed TEC (red curve), we can observe the effect of the flare on the ionospheric TEC, which is shown in Figure 8 (bottom). We may note a sudden increase in the ΔTEC similar

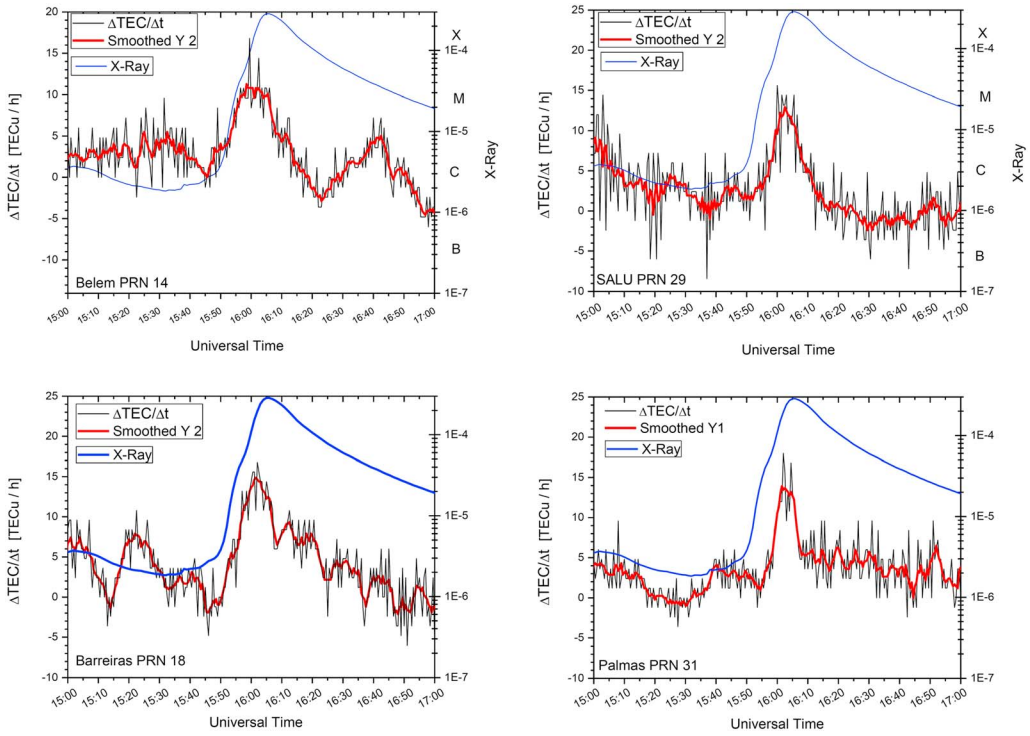

Figure 7. The TEC increase ratio given by ΔTEC/Δ*t* variation is shown for Belém, Palmas, Barreiras, and São Luís.

to that observed in Figure 5 (middle). We have also calculated the ΔTEC/Δt using the simulated TEC, and the results are shown in Figure 9, where we can observe that before the flare, our simulations were showing TEC increase ratio at about 4 TECU/h. However, when the flare started, the TEC increase ratio has instantaneously raised to values about 8 TECU/h, showing a remarkable increase in ΔTEC/Δt at the flare occurrence moment (16:00 UT), and finally returning to the previous intensity level. Comparing the results obtained from our theoretical calculations and the observations, we may observe that the SUPIM results are underestimating the observational results. Some possible causes for the differences between the model results and observations can be the inefficiency of the input parameters for zonal electric field, thermospheric neutral winds [see *Nogueira et al.*, 2013b], and the response of the neutral atmosphere densities to the solar flare [*Sutton et al.*, 2006]. The most pronounced deficiency of the present modeling is in the EUV flux for wavelengths larger than 40 nm, for which we had no enough data from EVE satellite to incorporate in our simulations. This part of the EUV flux enhancement is represented in our modeling by a simple addition of an increase of the EUV flux up to 10% of the baseline of *Tobiska et al.*'s [2000] model, which may not be sufficiently adequate.

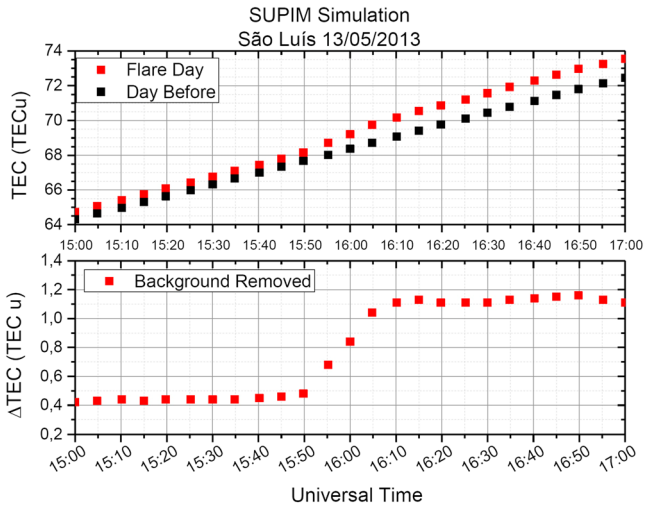

Figure 8. (top) TEC variation simulated by SUPIM, where the red line shows the TEC increases due to flare and the black line shows the simulation without the increased EUV flux (no flare condition). (bottom) The ΔTEC obtained by subtracting the background condition (black line) from the disturbed TEC (red line).

We used the SUPIM to investigate the time variation in the height versus

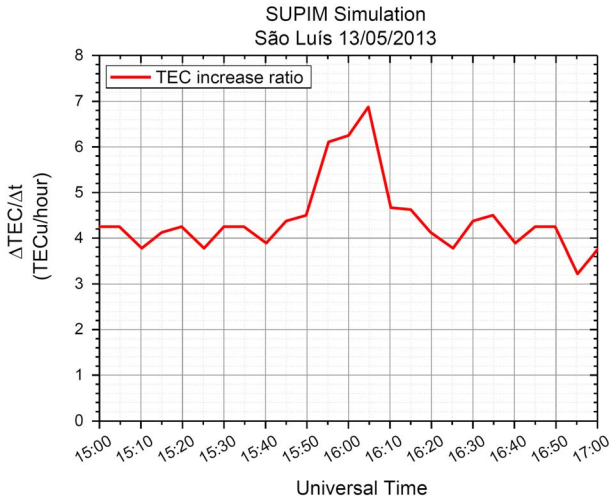

Figure 9. The theoretical TEC increase ratio given by $\Delta TEC/\Delta t$ variation for São Luís.

latitude distribution of the *F* region ionization in response to this X-class flare, seeking to understand the height-dependent ionospheric response to a solar flare. The model simulations were done by using as input the temporally varying solar flux from X-ray to EUV wavelengths. Based on calculations involving an extensive set of photochemical ionospheric reactions in the presence of dynamics and electrodynamics, the model provides the full spatial temporal evolution of the ionosphere buildup and recovery in response to the solar flare. Figure 10 presents the height versus latitude distribution of the excess electron density, ΔNe, obtained after removing the background density from the total density for successive intervals during the flare. We may note that at 14:55 UT, before solar flare (Figure 10a), there was no density enhancement in the equatorial and low-latitude ionosphere. However, just at the beginning of the solar flare (at 15:55 UT in Figure 10b), a significant increase in the electron density may be observed mainly in the ionospheric *E* region (around 100 km) and in the *F* region (around 200 km). The prompt increase in the *E* layer electron density must have been responsible for the sudden enhancement in Sq and EEJ current systems observed in Figures 2 and 4. Further, at higher up in the *F* region, the ionization enhancement has the pattern of the latitudinal structure of the equatorial ionization anomaly. The result at 16:25 UT, a few minutes after the solar flare initiation, presented in Figure 10c, shows a strong increase in the electron density near 250 km, which is near the *F* layer peak and that is displaced to latitude southward of the dip equator.

The features observed in Figure 10b, that is the large density increase at the ionospheric *E* region over the entire low-latitude region and the EIA structure of the ionization enhancement at higher *F* region altitudes, are due to the extra ionization by the flare-enhanced soft X-ray and EUV radiation. The relatively larger neutral density and photochemical processes lead to a rapid increase in the electron density at ~120 km. The dominant heavy ions (O_2^+ and NO^+) at these altitudes have a fast dissociative recombination rate, which caused the quick decrease in the electron density in this height region as can be noted in the ΔNe values being close to zero at ~120 km in the results at 16:25 UT. On the other hand, at higher altitudes, the dominance of the transport process over photochemical process, the lower neutral gas density, and less middle band EUV absorbed in the *F* region caused a slower increase in the ΔNe parameter at ~250 km to produce the results in Figure 10c. At the *F* region heights, the loss process of the dominant ion O^+ occurs mainly by ion-atom interchange reaction that is much slower compared with the dissociation recombination of the molecular ion, causing a slower decrease in the ΔNe at this altitude [see also *Le et al.*, 2007]. A remarkable

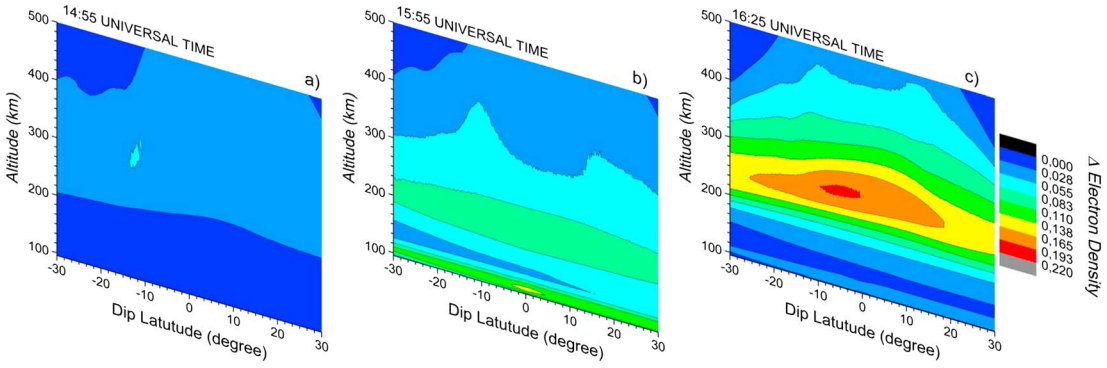

Figure 10. The temporal, latitudinal, and altitudinal dependence of the increased electron density due to the enhancement of EUV flux as obtained from SUPIM.

result of our simulations is the largest ionospheric increase occurring at approximately 7° negative dip latitude (Figure 10c), a behavior that is entirely in agreement with the observational result shown in Figure 6, wherein the highest ΔTEC disturbance was observed slightly off equator (~7° dip latitude).

4. Conclusion

In the present work, we have studied the effects of the strong solar flare of 13 May 2013 on the equatorial and low-latitude ionosphere over South America. We have presented and discussed the results in terms of the *D* and *E* region effects observed by Digisondes in Brazil and magnetometers in Brazil and Peru, as well as in terms of the responses of the TEC as observed by a network of GNNS receivers in South America. The results have permitted the characterization of the *D* region ionization enhancement that caused HF radio wave blackout at location separated in east-west direction as also the characterization of the EEJ and the Sq current system responses as observed by latitudinally distributed magnetometers.

As the main focus of this study, we have analyzed the TEC data in South America in order to understand the dynamics of the latitude-longitude distribution of the TEC in response to the flare time EUV enhancement. Additionally, using a theoretical ionospheric model, we were able to simulate the solar flare effect in the *E* and *F* regions of the equatorial ionosphere, with reasonable success to explain many important features of the TEC variations in the observational data. The main results of this study can be summarized as follows:

1. The ionospheric sounding observations at São Luís and Fortaleza show total to partial blackout of HF wave traces in ionogram for about 70 min, as a result of the flare-induced enhanced electron density in the *D* region. The beginning and the end of the flare effect seem to lead in time at the eastern location as compared to the western location. It is the first time that such an effect is being reported.
2. Sudden intensification of the Sq current system and the EEJ occurs as a result of the flare-induced prompt increase in the *E* layer electron density. The Sq current enhancement is characterized by a strong increase in the *H* component at equatorial and low latitudes and a drastic decrease at a midlatitude station. It is found that the Δ*H* increase due to the EEJ intensification is around 5 times higher than that of the Sq intensification.
3. The solar flare increase in the EUV fluxes causes an abrupt increase in the ionospheric TEC at equatorial and low-latitude regions. The latitudinal distribution of the TEC disturbance shows larger enhancement closer to the EIA crest region and smaller at equatorial and midlatitude stations.
4. The theoretical model results show that most of *Ne* enhancements responding to a flare occur in the *E* region (110 km) at the beginning of the flare and in the *F* region (250 km) just a few minutes later, when the electron density enhancement shows a latitudinal structuring indicating the development of a plasma fountain leading to EIA formation due to the flare-induced ionization.

Acknowledgments

P.A.B. Nogueira acknowledges the support from Fundação de Amparo a Pesquisa do Estado de São Paulo (FAPESP) (grant 2013/01924-1). M.A.A. acknowledges the support from the CNPq through the process: 303083/2011-5. We would like to thank NASA/SDO and the AIA, EVE, and HMI for making the SDO available at http://sdo.gsfc.nasa.gov/. We acknowledge the CELIAS/SEM experiment on the Solar Heliospheric Observatory (SOHO) spacecraft for the EUV emission flux available at http://www.usc.edu/dept/space_science/semdatafolder/sem-download.htm (SOHO is a joint European Space Agency, United States National Aeronautics and Space Administration mission). The Jicamarca Radio Observatory is a facility of the Instituto Geofisico del Peru operated with support from the NSF AGS-0905448 through Cornell University (see database at http://jro.igp.gob.pe/english/). We acknowledge the EMBRACE/INPE for the TEC-GNSS (based on RAMSAC, LISN, RBMC, and IGS observatories), magnetometer, and ionosonde data available at http://www2.inpe.br/climaespacial/en/index. We also would like to thank CRAAM/Mackenzie University group for the VLF data availability. C.M. Denardini thanks CNPq/MCTI (grant 305242/2011-3) and FAPESP (grant 2012/08445-9), and Cueva, R.Y.C. thanks FAPESP fellowship under project 2012/25396-1.

Michael Liemohn thanks the reviewers for their assistance in evaluating this paper.

References

Abdu, M. A. (2005), Equatorial ionosphere-thermosphere system: Electrodynamics and irregularities, *Adv. Space Res.*, *35*(5), 771–787, doi:10.1016/j.asr.2005.03.150.

Afraimovich, E. L., A. T. Altynsev, V. V. Grechnev, and L. A. Leonovich (2001), Ionospheric effects of the solar flares as deduced from global GPS network data, *Adv. Space Res.*, *27*, 1333–1338.

Bailey, G. J., and N. Balan (1996), Some modeling studies of the equatorial ionosphere using the Sheffield University Plasmasphere Ionosphere Model, *Adv. Space Res.*, *18*(6), 59–68.

Bailey, G. J., and R. Sellek (1990), A mathematical model of the Earth's plasmasphere and its application in a study of He^+ at $L = 3$, *Ann. Geophys.*, *8*(3), 171–189.

Bailey, G. J., R. J. Moffett, and J. A. Murphy (1978), Interhemispheric flow of thermal plasma in a closed magnetic flux tube at midlatitudes under sunspot minimum conditions, *Planet. Space Sci.*, *26*, 753–765.

Bailey, G. J., R. Sellek, and Y. Rippeth (1993), A modeling study of the equatorial topside ionosphere, *Ann. Geophys.*, *11*(4), 263–272.

Bailey, G. J., N. Balan, and Y. Z. Su (1997), The Sheffield University Ionosphere-Plasmasphere Model: A review, *J. Atmos. Sol. Terr. Phys.*, *59*(13), 1541–1552.

Benz, A. O. (2008), Flare observations, *Living Rev. Sol. Phys.*, *5*, 1, doi:10.12942/lrsp-2008-1.

Hedin, A. E., et al. (1996), Empirical wind model for the upper, middle, and lower atmosphere, *J. Atmos. Terr. Phys.*, *58*, 1421–1447.

Heelis, R. A. (2004), Electrodynamics in the low and middle latitude ionosphere: A tutorial, *J. Atmos. Sol. Terr. Phys.*, *66*, 825–838.

Le, H., L. Liu, B. Chen, J. Lei, X. Yue, and W. Wan (2007), Modeling the responses of the middle latitude ionosphere to solar flares, *J. Atmos. Sol. Terr. Phys.*, *69*, 1587–1598, doi:10.1016/j.jastp.2007.06.005.

Liu, J. Y., C. S. Chiu, and C. H. Lin (1996), The solar flare radiation responsible for sudden frequency deviation and geomagnetic fluctuation, *J. Geophys. Res.*, *101*, 10,855–10,862, doi:10.1029/95JA03676.

Liu, J. Y., C. H. Lin, Y. I. Chen, Y. C. Lin, T. W. Fang, C. H. Chen, Y. C. Chen, and J. J. Hwang (2006), Solar flare signatures of the ionospheric GPS total electron content, *J. Geophys. Res.*, *111*, A05308, doi:10.1029/2005JA011306.

Manju, G., and K. S. Viswanathan (2005), Response of the equatorial electrojet to solar flare related X-ray flux enhancement, *Earth Planets Space*, *57*, 231–242.

Manju, G., T. K. Pant, C. V. Devasia, S. Ravindran, and R. Sridharan (2009), Electrodynamical response of the Indian low-mid latitude ionosphere to the very large solar flare of 28 October 2003: A case study, *Ann. Geophys.*, *27*, 3853–3860, doi:10.5194/angeo-27-3853-2009.

Matsushita, S. (1969), Dynamo currents, winds, and electric fields, *Radio Sci.*, *4*, 771–780, doi:10.1029/RS004i009p00771.

Moldavanov, A. V. (2002), Theory of "crotchet" impulse component generation, *J. Phys. D Appl. Phys.*, *35*, 1311–18.

Nogueira, P. A. B., M. A. Abdu, J. R. Souza, I. S. Batista, G. J. Bailey, A. M. Santos, and H. Takahashi (2013a), Equatorial ionization anomaly development as studied by GPS TEC and f_0F_2 over Brazil: A comparison of observations with model results from SUPIM and IRI 2012, *J. Atmos. Sol. Terr. Phys.*, *104*, 45–54.

Nogueira, P. A. B., M. A. Abdu, J. R. Souza, G. J. Bailey, I. S. Batista, E. B. Shume, and C. M. Denardini (2013b), Longitudinal variation in Global Navigation Satellite Systems TEC and topside ion density over South American sector associated with the four-peaked wave structures, *J. Geophys. Res. Space Physics*, *118*, 7940–7953, doi:10.1002/2013JA019266.

Otsuka, Y., T. Ogawa, A. Saito, T. Tsugawa, S. Fukao, and S. Miyazaki (2002), A new technique for mapping of total electron content using GPS network in Japan, *Earth Planets Space*, *54*, 63–70.

Picone J. M., A. E. Hedin, D. P. Drob, and A. C. Aikin (2002), NRLMSISE-00 empirical model of the atmosphere: Statistical comparisons and scientific issues, *J. Geophys. Res.*, *107*(A12), 1468, doi:10.1029/2002JA009430.

Qian, L., A. Burns, P. C. Chamberlin, and S. C. Solomon (2010), Flare location on the solar disk: Modeling the thermosphere and ionosphere response, *J. Geophys. Res.*, *115*, A09311, doi:10.1029/2009JA015225.

Qian, L., A. G. Burns, S. C. Solomon, and P. C. Chamberlin (2012), Solar flare impacts on ionospheric electrodyamics, *Geophys. Res. Lett.*, *39*, L06101, doi:10.1029/2012GL051102.

Rangarajan, G. K., and R. G. Rastogi (1981), Solar flare effect in equatorial magnetic field during morning counter electrojet, *Ind. J. Rad. Space Phys.*, *10*, 190–192.

Rastogi, R. G., B. M. Pathan, D. R. K. Rao, T. S. Sastry, and J. H. Sastri (1999), Solar flare effects on the geomagnetic elements during normal and counter electrojet periods, *Earth Planets Space*, *51*, 947–957.

Raulin, J. P., G. Trottet, M. Kretzschmar, E. L. Macotela, A. Pacini, F. C. P. Bertoni, and I. E. Dammasch (2013), Response of the low ionosphere to X-ray and Lyman α solar flare emissions, *J. Geophys. Res. Space Physics*, *118*, 570–575, doi:10.1029/2012JA017916.

Richmond, A. D. (1995), Modeling equatorial ionospheric electric fields, *J. Atmos. Terr. Phys.*, *57*(10), 1103–1115, doi:10.1016/0021-9169(94)00126-9.

Sahai, Y., F. Becker-Guedes, P. R. Fagundes, W. L. C. Lima, A. J. de Abreu, F. L. Guarnieri, C. M. N. Candido, and V. G. Pillat (2006), Unusual ionospheric effects observed during the intense 28 October 2003 solar flare in the Brazilian sector, *Ann. Geophys.*, *25*, 2497–2502.

Scherliess, L., and B. G. Fejer (1999), Radar and satellite global equatorial *F* region vertical drift model, *J. Geophys. Res.*, *104*, 6829–6842, doi:10.1029/1999JA900025.

Souza, J. R., M. A. Abdu, I. S. Batista, and G. J. Bailey (2000), Determination of vertical plasma drift and meridional wind using the Sheffield University Plasmasphere Ionosphere Model and ionospheric data at equatorial and low latitudes in Brazil: Summer solar minimum and maximum conditions, *J. Geophys. Res.*, *105*, 12,813–12,821, doi:10.1029/1999JA000348.

Sripathi, S., N. Balachandran, B. Veenadhari, R. Singh, and K. Emperumal (2013), Response of the equatorial and low-latitude ionosphere to an intense X-class solar flare (X7/2B) as observed on 09 August 2011, *J. Geophys. Res. Space Physics*, *118*, 2648–2659, doi:10.1002/jgra.50267.

Sutton, E. K., J. M. Forbes, R. S. Nerem, and T. N. Woods (2006), Neutral density response to the solar flares of October and November 2003, *Geophys. Res. Lett.*, *33*, L22101, doi:10.1029/2006GL027737.

Thome, G. D., and L. S. Wagner (1971), Electron density enhancements in the *E* and *F* regions of the ionosphere during solar flares, *J. Geophys. Res.*, *76*, 6883–6895, doi:10.1029/JA076i028p06883.

Thomson, N. R., and M. A. Clilverd (2001), Solar flare-induced ionospheric *D* region enhancements from VLF amplitude observations, *J. Atmos. Sol. Terr. Phys.*, *63*, 1729–1737.

Thomson, N. R., C. J. Rodger, and R. L. Dowden (2004), Ionosphere gives size of greatest solar flare, *Geophys. Res. Lett.*, *31*, L06803, doi:10.1029/2003GL019345.

Tobiska, W. K., T. Woods, F. Eparvier, R. Viereck, L. Flyod, D. Bouwer, G. Rottman, and O. R. White (2000), The SOLAR2000 empirical solar irradiance model and forecast tool, *J. Atmos. Terr. Phys.*, *62*, 1233–1250.

Tsurutani, B. T., et al. (2005), The October 28, 2003 extreme EUV solar flare and resultant extreme ionospheric effects: Comparison to other Halloween events and the Bastille Day event, *Geophys. Res. Lett.*, *32*, L03S09, doi:10.1029/2004GL021475.

Van Sabben, D. (1968), Solar flare effects and simultaneous magnetic daily variation, *J. Atmos. Terr. Phys.*, *30*, 1641–1648.

Woods, T. N., et al. (2010), Extreme Ultraviolet Variability Experiment (EVE) on the Solar Dynamics Observatory (SDO): Overview of science objectives, instrument design, data products, and model developments, *Sol. Phys.*, *275*, 115–143, doi:10.1007/s11207-009-9487-6.

Xiong, B., et al. (2011), Ionospheric response to the X-class solar flare on 7 September 2005, *J. Geophys. Res.*, *116*, A11317, doi:10.1029/2011JA016961.